Nuclear Materials and Energy 12 (2017) 518–523

Contents lists available at ScienceDirect

Nuclear Materials and Energy

journal homepage: www.elsevier.com/locate/nme

Whole-machine material migration studies in the TEXTOR tokamak with molybdenum

A. Weckmann[a,*], P. Petersson[a], A. Kirschner[b], P. Wienhold[b], S. Brezinsek[b], A. Kreter[b], A. Pospieszczyk[b], M. Rubel[a]

[a] Fusion Plasma Physics, Royal Institute of Technology (KTH), 100 44 Stockholm, Sweden
[b] Institute for Energy and Climate Research (IEK-4, Plasma Physics), Forschungszentrum Jülich, 52425 Jülich, Germany

ARTICLE INFO

Article history:
Received 15 July 2016
Revised 23 November 2016
Accepted 9 December 2016
Available online 27 December 2016

Keywords:
Global transport
Material migration
High-Z metals
TEXTOR
Plasma-facing components
Molybdenum

ABSTRACT

MoF_6 injection from a localised source into plasma edge in the TEXTOR tokamak was the last experiment before the final shut-down of the TEXTOR machine. During decommissioning all plasma-facing components (PFCs) became available for surface studies. Detailed mapping of Mo deposition was performed in order to determine its migration on global scale. The concentration of Mo on PFC decays exponentially with distance from the source. The decay length is of the order of 0.1 m on the main PFC and 1 m on the receded components. Also the decay lengths modelled with the ERO code are between 0.15–1.3 m, depending on the anomalous cross-field diffusion coefficient. The inner bumper limiter is found to be the major repository for Mo. Material balance measurements show that only up to 22% of the injected Mo was detected on all the PFCs thus indicating that a large fraction of injected Mo may have been pumped out before being deposited.

1. Introduction

High-Z metals are extensively studied in fusion devices to assess their performance under ITER relevant conditions [1–3]. The scope is to minimise the fuel accumulation, especially with tritium, via suitable wall material selection for ITER [4,5]. Tungsten is considered the most adequate plasma-facing material (PFM), tolerating high heat fluxes, having low physical sputtering yields and very low fuel accumulation [6]. On the other hand, W has a strong poisoning effect on the core plasma [7], and under reactor relevant conditions it is also eroded [5]. Bearing this in mind, understanding high-Z transport in general and W transport in particular is a key issue for future fusion devices.

The term transport in fusion devices is often separated into local and global transport. Local transport means that an impurity does not enter the main plasma and is therefore mostly deposited in the vicinity of its origin [8]. This can happen by different processes like prompt re-deposition [9,10] or screening [11]. For global transport an impurity is deposited outside the region of origin, e.g. on neighbouring tiles or completely different parts of the machine. Due to the strong plasma poisoning effect of high-Z materials, local transport and deposition is favoured, where the high-Z materials have only minimal probability to enter the main plasma. Additionally, very localised transport, e.g. by prompt re-deposition, could limit gross erosion and thus extend the lifetime of plasma facing components (PFCs).

Material migration experiments, using tracers to identify deliberately released material, showed that only a minor fraction undergoes local deposition [12–14]. The reason is that re-deposited material is easy to re-erode and therefore can be transported long distances by stepwise erosion-deposition processes [13,15]. In operating machines it is only possible to extract a few PFCs for deposition studies, and therefore the knowledge on detailed deposition patterns on a whole-machine scale is limited. The final shut-down of TEXTOR in 2013 provided the unique possibility to extract as many PFCs as needed for a detailed deposition mapping. The last experiment in TEXTOR was thus a tracer experiment, using Mo as tracer for W because tungsten had been used in previous transport experiments. Molybdenum was released into the machine via its hexafluoride, MoF_6, in a local injection, creating a well-defined source of Mo. In the following, a large number of PFCs was retrieved for ex-situ studies with ion beams. Simulations of the well-developed code ERO [16] was employed in order to understand the found deposition patterns. Local deposition results have already been published in [17].

* Corresponding author.
E-mail address: weckmann@kth.se (A. Weckmann).

http://dx.doi.org/10.1016/j.nme.2016.12.011

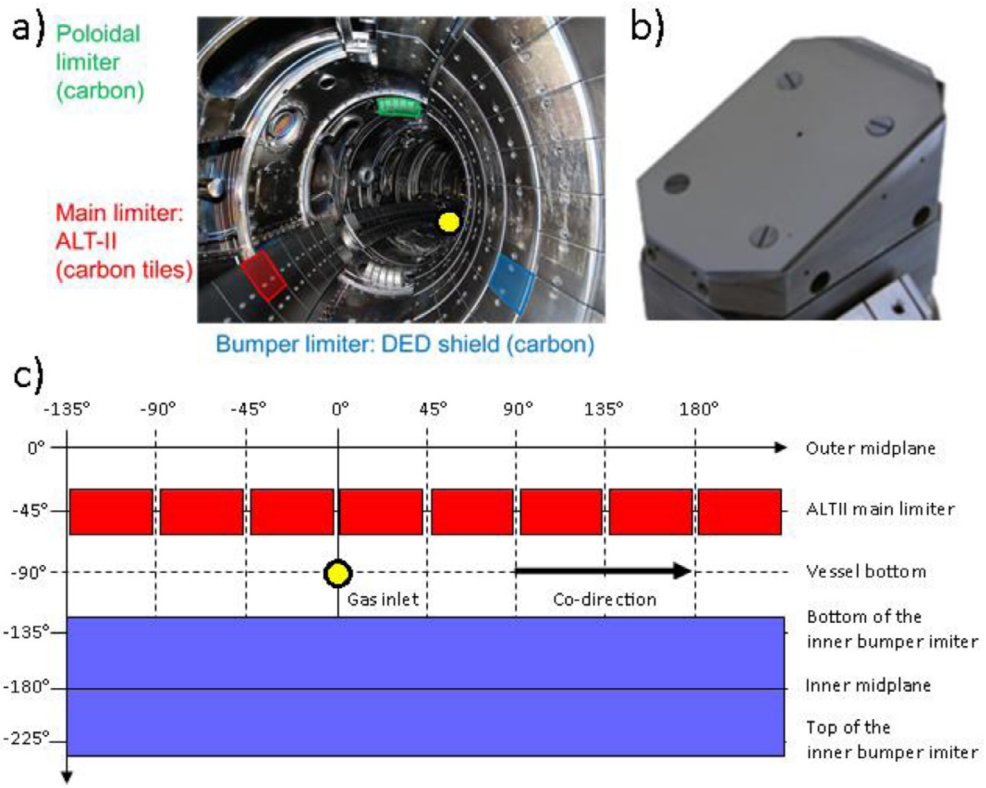

Fig. 1. Schematic view on all analysed PFCs and wall probes: a) Photograph of TEXTOR interior with ALTII main limiter (red), inner bumper limiter (blue), poloidal limiter (green), and injection point (yellow circle); b) detail of the injection point: the single roof limiter; c) display of the PFCs unfolded in the toroidal-poloidal plane with the limiters displayed in Fig. 3: ALTII limiter (red) and inner bumper limiter (blue). (For interpretation of the references to colour in this figure legend, the reader is referred to the web version of this article.)

In this paper, a detailed whole-vessel mapping of the deposited high-Z material Mo will be shown, alongside with ERO simulations reproducing the found patterns in a qualitative way via a simplified geometry with TEXTOR-relevant plasma parameters. More details of ERO modelling of Mo transport are given in [18].

2. Experimental

The TEXTOR tokamak was a medium-size machine with major radius $R = 1.75$ m and minor plasma radius $a = 0.46$ m, defined by the main PFC, the ALTII limiter [19]. Other important PFCs were the inner bumper limiter at $r = 0.49$ m [20] and the movable poloidal limiter [21] situated at $r = 0.48$ m during this experiment. All PFCs were made from carbon. The PFCs discussed in this paper are shown in Fig. 1, where co-direction indicates the direction of the plasma current and counter-direction the opposite.

The Inconel 625 liner was routinely heated up to 250 °C for outgassing [21] and was located at $r = 0.546$ m [22]. More experimental details can be found in [17].

The injection of MoF_6 during this experiment took place through a single roof test limiter [23] located at the bottom of the vessel in front of a viewing system described in [24] to monitor the injection. The injection was performed during 31 discharges in the flat-top phase. In total, 5.7×10^{20} Mo atoms were injected, which was measured by transforming the MoI line intensity at 388 nm to absolute amounts via so called "S/XB values" [25]. A more detailed discussion is given in [17]. The integrated plasma time was 201.5 s.

After the experiment, in total 136 tiles were removed for global studies from the main PFC, ALTII, and the inner bumper limiter. For the first time, the inner bumper limiter was subject to an extensive tile surface study with ion beam analysis. Additionally poloidal limiter PFCs were studied but will not enter in this paper due to low Mo concentration on their surface and hence insignificance to the overall pattern. More details are listed in Table 1. For assessment of background Mo levels, tiles removed before the experiment were analysed.

Table 1
Amount of analysed PFCs and liner parts for this study, with means of analysis.

PFC (all carbon)	Analysed PFC surface	Ion beam analysis
ALT main limiter	17% of total surface	RBS, ToF ERDA
Bumper limiter	15% of total surface	RBS, ToF ERDA
Poloidal limiter	60% of total surface	RBS
Collector probe	25% of exposed samples	RBS
Liner	8 locations	ToF ERDA

Two different ion beam analysis methods were carried out for Mo quantification, namely Rutherford Backscattering Spectroscopy (RBS) with 2 MeV $^4He^{2+}$, and a time-of-flight Elastic Recoil Detection Analysis (ToF ERDA) with 36 MeV $^{127}I^{8+}$. Quantification of Mo was a key issue for this experiment, and hence a lot of effort was taken to compensate the weaknesses of RBS with the strength of ERDA and vice-versa. RBS suffered from signal convolution and could only probe to a depth of approximately 200 nm before the Mo signal was covered by the stronger Inconel signal, while the layer built up during this experiment had a minimum thickness of 300 nm, assuming 1–3 nm/s deposition rate as commonly experienced in TEXTOR [26,27]. The drawback could be overcome by extrapolating RBS depth profiles and comparing the gross Mo amount with those obtained with ERDA, which could probe up to a depth of 500 nm without convolution problems. On the other hand, ERDA signals suffer from surface roughness effects due to glancing incidence and scatter angles, while RBS does not have this prob-

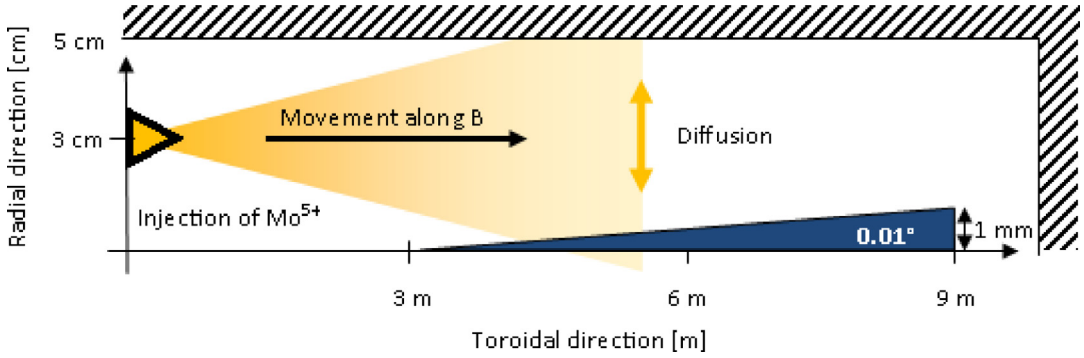

Fig. 2. Geometry of the global ERO simulation. The hatched areas represent the boundaries of the simulation box at height 5 cm and length 10 m. x and y axes have different units: m and cm, respectively, for better visibility.

lem due to head-on beam and detection geometry. Here, comparison of the Mo content in the first 200 nm between ERDA and RBS was applied with the Pearson product-moment correlation coefficient (PPMCC), which measures the correlation between two sets of data points. Thus it was ensured that the surface roughness effects do not de-correlate the ERDA results for Mo content from the real Mo content on the probed surface. Apart from the cross-check, subtraction of background Mo concentration from previous experiments and the Inconel liner had to be performed. This was done by measuring three tiles of the main PFC, the ALTII limiter, and three more tiles of the inner bumper limiter.

Finally, simulations in a simplified geometry were employed with the ERO code [16,18]. The goal here was to study, if one can reach qualitative agreement between simulation and experiment in order to motivate more comprehensive simulations of this experiment in the future and also promote the found results for code benchmarking. Typical TEXTOR plasma parameters for neutral beam plasmas were applied for the simulation: a magnetic field of 2.25 T at grazing incidence on the PFC (0.01°), electron temperature T_e of 30 eV, electron density n_e of 5×10^{12} cm^{-3} with 40 mm as radial exponential decay length, background plasma flow velocity v_{flow} of 1×10^4 m/s along the toroidal direction. A cross-field diffusion coefficient of $D_{perp} = 0.2$ m^{2}s^{-1} was assumed as standard [28,29], while ten times lower diffusion coefficient was used for parameter studies. The sound velocity for the assumed plasma parameters is 5×10^4 m/s. 1000,000 particles were traced in the simulation, where tracing ended when the particle either left the simulation volume or was deposited on the PFC. Simulated particles were Mo^{5+} ions as a simple approach to the mixed Mo charge states that may be found near the PFCs with T_e of the order of 30 eV – ionisation potential of Mo^{4+} is 46 eV, for Mo^{5+} it is 55 eV, and for Mo^{6+} 69 eV. During the real experiment, the Mo was injected radially into the SOL plasma and had to be transported around the injection limiter before being transported in co direction (see Fig. 4 in [17]). To allow for SOL transport without complicating the simulation, the particle source is modelled 3 m away from the PFC in toroidal direction and 3 cm in radial direction. The geometry simulated with ERO is shown in Fig. 2.

3. Results and discussion

3.1. Material balance

The Mo background found on tiles extracted before this experiments results from previous experiments and the TEXTOR Inconel liner. It is on average 0.8×10^{15} cm^{-2} on the ALTII limiter and 0.6×10^{15} cm^{-2} on the bumper limiter. These values are comparable to the Mo concentrations found after this experiment on the ALTII and inner bumper limiters. Hence a homogeneous distribution of the injected Mo throughout the whole machine with subsequent increase of Mo could not be detected. In the further analysis, the found Mo background was subtracted from the found concentration in order to present the numbers for injected Mo only.

Table 2 lists the integrated quantities of Mo found on different PFCs. Fig. 3 shows the obtained pattern. As it can be seen on the ALTII limiter the Mo concentration shows a strong gradient: The tiles closest to the injection point exhibit the highest Mo concentration, while already neighbouring tiles had much lower Mo concentration. Hence the ALTII tiles adjacent to the injection point were used to calculate a “injection area average” multiplied only with the area covered by these adjacent tiles. All other tiles had much lower concentration – their average was taken separately and multiplied by their area. In either case, an extrapolation of existing Mo levels according to 1–3 nm/s deposition rate was adopted for RBS results. With RBS one thus finds 1–2% of injected Mo, and 2% with ERDA, after background subtraction. Cross-checking Mo surface concentration (first 200 nm) of ERDA and RBS yields a PPMCC = 0.99, hence despite the rough carbon substrate the ERDA results have not been deteriorated significantly by roughness effects.

On the inner bumper limiter, 3 cm behind the LCFS, tiles revealed dim grey to shiny colourful deposits under visual inspection in contrast to the mostly dull grey ALTII tiles. Also here, RBS and ERDA data up to 200 nm show good correlation with a PPMCC = 0.95. Extrapolating RBS results beyond 200 nm gives 7–10% of injected Mo, while ERDA measurements yield 11% after background subtraction. The uncertainties are 1/5 of the obtained values, i.e. between 1.4% and 2.2%. Hence within the uncertainties RBS and ERDA agree well.

From previous studies published in [17] the amount deposited directly around the gas inlet amounts to 6% ± 1% while other places like tile sides and the liner prove to be of no importance for the Mo balance. Previous studies showed low deposition rates on the liner [30]. Only the deposition on the poloidal limiter may be considered: up to 1% of injected Mo. Proper measurements on the poloidal limiter are hampered by the limiter tile geometry, making proper alignment difficult, and thick flaky deposits from years of operation. The poloidal limiter extended radially and no Mo background concentration is available for these positions, hence no proper Mo background subtraction could be performed for the poloidal limiter. The mentioned 1% is thus an upper estimate.

The total amount of injected Mo on all examined PFCs is then between 15 and 20% of the Mo amount that entered the vessel. The Mo balance could hence not been closed, although considerable effort was taken in locating it also in recessed areas like tile sides and the liner. On tile sides right next to the injection point the integrated Mo amount is in *per mille* range and hence negligible. On the liner, the deposited layer thickness during the ex-

Table 2
Amount of Mo found on analysed PFCs and LL1, relative to the injected amount of MoF_6, and peak concentration. More details on local Mo deposition and LL1 analysis can be found in [13].

PFC, machine parts	Amount of Mo rel. to injected Mo amount [%]	Max. Mo surface concentration [10^{15}/cm^2]
ALT main limiter	1 ± 0.2 (RBS) – 2 ± 0.4 (ERDA)	4.8
Bumper limiter	7 ± 1.4 (RBS) – 11 ± 2.2 (ERDA)	4.7
LL1 cover plate	6 ± 1 [13]	12 000 (details in [13])
Poloidal limiter	≤1	5.4
Collector probe	0.02	10.2
Liner (extrapol.)	≤2	0.2 (in the topmost 5 nm)

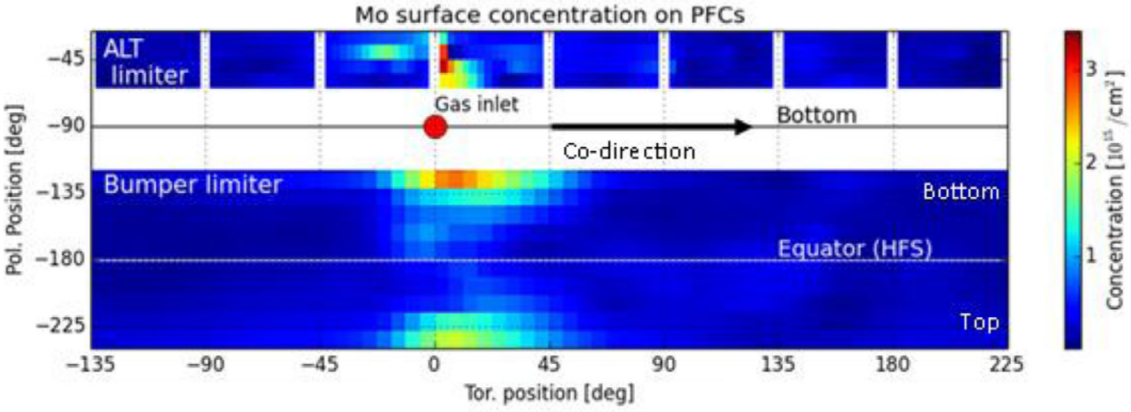

Fig. 3. Interpolation of Mo surface concentration measurements with RBS, in 10^{15} cm^{-2}. For visualisation the PFC surfaces have been projected into φ-θ plane, with $\theta = 0$ at the low-field side and $\theta = -180$ on the high-field side (HFS).

periment should be in the range of a few nm according to Seggern et al. [30]. Assuming 5 nm deposition as upper boundary, and averaging the Mo content on all measured liner pieces in this topmost layer, one obtains 4×10^{13} cm^{-2} Mo concentration as upper estimate. Multiplying this number with the torus area minus the PFC area, about 257,000 cm^2 together with the port holes, one obtains 0.1×10^{20} Mo atoms or 1.8% of the injected Mo as upper estimate for the deposition on the liner. This shows that the liner, port holes and other recessed areas can play a minor role in the material balance due to size. However, the obtained amount is comparable to the Mo uncertainty for the inner bumper limiter.

The only large sink left is the pumping system, hence Mo may have been pumped out in some gaseous form. No analysis on the pumps has been possible though, and the Mo balance must remain unclosed.

Since Mo concentration falls off to background levels further away from the injection point, no homogeneous deposition could be clearly identified. The deposition on nearby limiters and the vicinity of injection show exponential decay behaviour. Average concentration on the ALTII limiter is $2.0–2.9 \times 10^{14}$ cm^{-2}; on the inner bumper limiter it is $4.6–6.9 \times 10^{14}$ cm^{-2}. One thus finds an overall higher concentration on the bumper limiter, implying that the injected Mo was preferably transported to the recessed inner bumper limiter. Exponential decay was also observed in radial direction, measured with a collector probe, with 1.1 cm decay length in co-direction and 2.9 cm in counter-direction.

3.2. Deposition pattern and ERO modelling

Two disruptions took place during the experiment; the later one occurred ten discharges before final shutdown. Hence in the following, the discussion will focus on the very top Mo resulting from the last five to ten discharges of the experiment (top 50–150 nm) experiencing quiescent plasma. The Mo concentration of more than 570 RBS measurements was interpolated with linear radial basis functions and plotted in Fig. 3.

Table 3
Exponential decay lengths of global Mo and W patterns in toroidal and poloidal direction, based on linear interpolations.

PFC	Decay length – Mo [cm]	
Toroidal direction	**Co**	**Counter**
ALT limiter	12 ± 5	26 ± 7
Bumper limiter		
Top	103 ± 21	66 ± 14
Bottom	105 ± 21	84 ± 18
Poloidal direction	**Top**	**Bottom**
Bumper limiter	20 ± 4	15 ± 3

As mentioned above, the Mo concentration falls off to background levels in an exponential way, both on the ALTII main limiter and the inner bumper limiter. This is in accordance with previous findings [13,31]. Decay lengths are given in Table 3. However, large variations on tiles adjacent to the injection point occur on small scale and decay lengths in Table 3 are not applicable directly next to the injection point. Uncertainties for the decay lengths are based on uncertainty of the ion beam data, ca. 1/5 of the measured concentration, and ambiguity in evaluating the patterns, but do not account for the aforementioned small scale variations close to the injection point. Due to the exponential decay, Mo deposition is located around the injection zone, about ±15° toroidally, with predominant deposition in co-direction. The maximum Mo concentration on the ALTII limiter is 4.8×10^{15} cm^{-2} in the vicinity of the injection point. On the inner bumper limiter, the maximum concentration is 4.7×10^{15} cm^{-2}. However, the following features do not fit in the exponential decay scheme: First, on the ALTII limiter (Fig. 3, x|y coordinates: −20|−45), Mo concentration peaks despite its distance to the injection point. Visual inspection showed strongly localised metallic deposits consisting of an alloy containing Mo and lighter metals. It is speculated that it originates from molten debris, but its origin and time of deposition remains unclear. Second, on the upper part of the inner bumper limiter (Fig. 3,

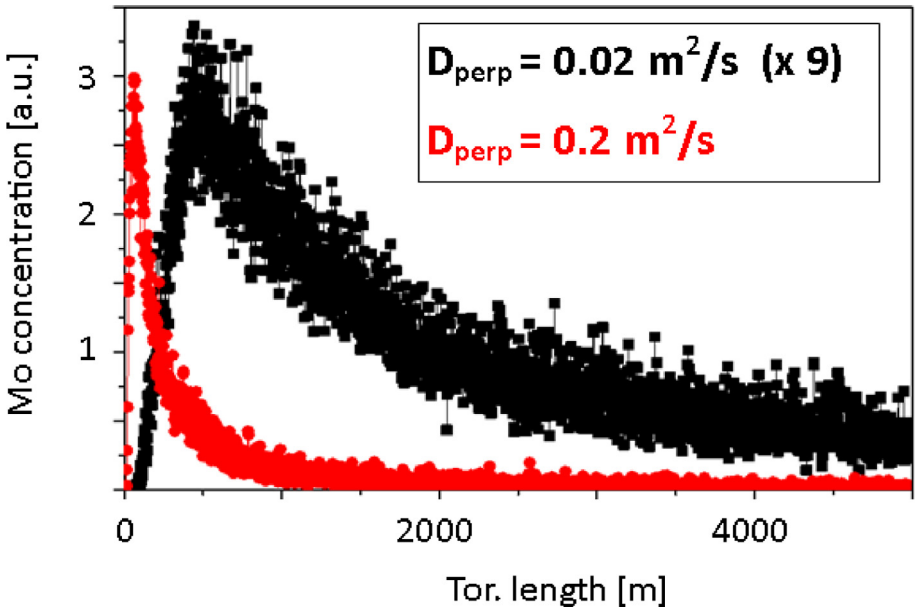

Fig. 4. ERO simulation of global deposition, toroidal pattern. The curve for $D_{perp} = 0.02\ m^2 s^{-1}$ is scaled by a factor 9 for better visibility.

x|y coordinates: +20|−240), Mo concentration is very high despite its large poloidal distance from the injection point. This observation will be discussed in Section 3.3.

In order to understand the obtained deposition pattern, global modelling must be employed, i.e. with simulation volumes extending beyond the vicinity of impurity origin. As a first step, ERO simulations with increased simulation volume were conducted, reproducing the found exponential decay and hence encouraging more sophisticated modelling. The found decay length is 15 cm and thus close to the experimentally obtained value of 12 cm for the ALTII limiter. Decreasing the cross-field diffusion coefficient to $D_{perp} = 0.02\ m^2 s^{-1}$ results in an increased decay length of 130 cm, which is closer to the value of around 1 m found on the bumper limiter. The simulated deposition profiles are shown in Fig. 4, with a nine fold magnification of the $D_{perp} = 0.02\ m^2/s$ curve. Deposition efficiencies are about 60% for $D_{perp} = 0.02\ m^2/s$ and 84% for $D_{perp} = 0.2\ m^2/s$, without re-erosion. Since the measured deposition efficiencies are considerably lower – on the order of *per mille* – re-erosion must play an important role in the overall obtained deposition pattern and material balance. On the other hand, despite the missing re-erosion process in the simulation an exponential profile could be obtained, suggesting that it is not the re-erosion-re-deposition process that leads to an exponential decay in Mo concentration. A possible explanation for the exponential decay is thus due to cross-field diffusion, where the field lines project the radial diffusion profile of Mo on the PFC when intersecting it.

3.3. Influence of flows on the deposition pattern

The Mo concentrations on the ALTII limiter and inner bumper limiter bottom are shifted by 5° or 15 cm toroidally in co direction, implying transport of the whole Mo "cloud" after injection. In addition, the Mo pattern in Fig. 3 seems to be shifted towards the inboard side, which is the $E \times B$ drift direction. The same trend also appears in the vicinity of the injection point [17], indicating that drift based SOL flows may influence the point of first deposition after which re-erosion-re-deposition processes smear out the pattern further. What seems odd is that the point of highest Mo concentration is not closest to the injection point, but actually "above" it in positive poloidal direction – but this can possibly explained again with the flow pattern found in [32]. Therein, the flow close to the LCFS is in positive poloidal direction with about 4000 m/s, then it reverses to circa 1300 m/s in negative poloidal direction. For the radially outward diffusing Mo this flow pattern would lead to a "zick-zack" trace together with the toroidal plasma flow – first towards the ALTII limiter, then towards the recessed bumper limiter, which is in fact observed. Mo that did not diffuse outward into the reversed flow region would have traversed around the short circumference and ended on the upper part of the inner bumper limiter, which is also observed. Unfortunately, the transport due to flow can only be discussed on qualitative level since there was no measurement of flow velocities for this experiment, and the values given in [32] had been obtained before a major refurbishment in TEXTOR. Nevertheless, the hitherto mentioned hints indicate that detailed knowledge of flows and drifts significantly helps to understand deposition patterns.

4. Concluding remarks

The major contribution of this work to material migration studies in tokamaks is related to a very comprehensive evaluation of PFCs on a global scale. Such a large dataset based on quantitative, depth profiling and ppm sensitive ion beam analysis has been obtained for the very first time. The usage of a well-defined source of marker element Mo under stable plasma conditions made it possible to investigate deposition patterns as developed during quiescent plasma operation. Together with background evaluation, even quantification was possible. The findings suggest that flows determine the position of first deposition, while comparison with ERO simulations suggest diffusion processes as reason for the exponential decay. Decay lengths are in the order between 0.1 m and 1 m, depending on PFC and direction (co- or counter).

However, despite dense mapping of the major PFCs and analysis of minor PFCs and the liner, at least 80% of the injected Mo remains lost and the balance could not be closed. This is a common situation for marker experiments, e.g. [33,34]. As the only other big sink during the experiment were the constantly running pumps underneath ALTII it is suggested that the Mo species were pumped out. However, the analysis of the pumping system was not possible.

This work has an impact on future activities encompassing both modelling and material analysis. Simulations using ERO agree well

with the findings on the ALTII main limiter, thus encouraging further effort in global modelling. Very detailed analyses performed for the first time on the inner bumper limiter tiles have indicated high concentration of deposited Mo (and also fuel species) in that recessed area. This, in turn, calls for enhanced efforts in the examination of the inner wall structures, e.g. inner wall cladding tiles in JET.

Acknowledgements

This work has been carried out within the framework of the EUROfusion Consortium and has received funding from the Euratom Research and Training Programme 2014–2018 under grant agreement No 633053. The views and opinions expressed herein do not necessarily reflect those of the European Commission. The work has been partly funded by the Swedish Research Council (VR) through contracts no. 621-2012-4148 and 2015-04844. All ion beam analysis was conducted in the Ion Technology Centre, Uppsala University, Sweden and is therefore highly acknowledged. From the TEXTOR team in Jülich, Jan W. Coenen and Michael Rack are acknowledged for providing spectroscopic results, and operating the collector probe. Antti Hakola provided helpful suggestions. Petter Ström, Oskar Eliasson and Pavel Kupsc helped with ion beam analysis of PFC and collector probe. Jury Romanzanov provided helpful comments regarding interpolation.

References

[1] G.F. Matthews, et al., JET ITER-like wall – overview and experimental programme, Phys. Scr. T145 (2011).
[2] R. Neu, Overview on plasma operation with a full tungsten wall in ASDEX Upgrade, J. Nucl. Mater. 438 (2013) 34–41.
[3] C. Bourdelle, et al., WEST physics basis, Nucl. Fusion 55 (2015).
[4] ITER Organisation, The ITER Tokamak, 2016 http://www.iter.org/mach (accessed March 2016).
[5] J. Roth, et al., Recent analysis of key plasma wall interaction issues for ITER, J. Nucl. Mater. 390-391 (2009) 1–9.
[6] V. Philipps, Tungsten as material for plasma-facing components in fusion devices, J. Nucl. Mater. 415 (2011) S2–S9.
[7] M.Z. Tokar, et al., Nature of high-Z impurity accumulation in tokamaks, Nucl. Fusion 37 (1997) 1691–1708.
[8] V. Philipps, P. Wienhold, A. Kirschner, M. Rubel, Erosion and redeposition of wall materials in controlled fusion devices, Vacuum 67 (2002) 399–408.
[9] D. Naujoks, R. Behrisch, Erosion and redeposition at the vessel walls in fusion devices, J. Nucl. Mater. 220-222 (1995) 227–230.
[10] D. Naujoks, et al., Tungsten as target material in fusion devices, Nucl. Fusion. 36 (1996) 671–687.
[11] J.D. Strachan, et al., JET carbon screening experiments using methane gas puffing and its relation to intrinsic carbon impurities, Nucl. Fusion 43 (2003) 922–941.
[12] M. Rubel, et al., Tracer techniques for the assessment of material migration and surface modification of plasma-facing components, J. Nucl. Mater. 463 (2015) 280–284.
[13] W.R. Wampler, et al., Measurements of net erosion and redeposition of molybdenum in DIII-D, J. Nucl. Mater. 438 (2013) 822–826.
[14] M. Rubel, et al., Tungsten migration studies by controlled injection of volatile compounds, J. Nucl. Mater. 438 (2013) 170–174.
[15] S. Brezinsek, et al., Quantification of tungsten sputtering at W/C twin limiters in TEXTOR with the aid of local WF6 injection, Phys. Scr. T145 (2011).
[16] A. Kirschner, et al., Simulation of the plasma-wall interaction in a tokamak with the Monte Carlo code ERO-TEXTOR, Nucl. Fusion 40 (2000) 989–1001.
[17] A. Weckmann, et al., Local migration studies of high-Z metals in the TEXTOR tokamak, Phys. Scr. T167 (2015) 014058.
[18] A. Kirschner et al., Modelling of deposition and erosion of injected WF6 and MoF6 in TEXTOR, this volume.
[19] R.W. Conn, et al., The toroidal belt pump limiter, ALT-II, in the TEXTOR tokamak, Fusion Eng. Des. 13 (1990) 251–259.
[20] B. Giesen, et al., Technical lay-out of the dynamic ergodic divertor, Fusion Eng. Des. 37 (1997) 341–346.
[21] O. Neubauer, et al., Design features of the tokamak TEXTOR, Fusion Sci. Technol. 47 (2005) 76–86.
[22] W. Kohlhaas, C. Stickelmann, B. Brandt, F. Durodié, New liner and ICRH antennae; Integration of ALT-II in TEXTOR, Fusion Eng. Des. 13 (1990) 321–336.
[23] A. Kreter, et al., Study of local carbon transport on graphite, tungsten and molybdenum test limiters in TEXTOR by (CH4)-C-13 tracer injection, J. Nucl. Mater. 363 (2007) 179–183.
[24] S. Brezinsek, et al., Characterization of deuterium recycling flux in front of a graphite surface in the TEXTOR tokamak, Plasma Phys. Contr. F. 47 (2005) 615–634.
[25] A. Pospieszczyk, et al., Determination of rate coefficients for fusion-relevant atoms and molecules by modelling and measurement in the boundary layer of TEXTOR, J. Phys. B 43 (2010).
[26] M. Mayer, et al., Hydrogen inventories in nuclear fusion devices, J. Nucl. Mater. 290-293 (2001) 381–388.
[27] M. Rubel, P. Wienhold, D. Hildebrandt, Fuel accumulation in co-deposited layers on plasma facing components, J. Nucl. Mater. 290-293 (2001) 473–477.
[28] D. Naujoks, Plasma-Material Interaction in Controlled Fusion, Springer-Verlag, Berlin Heidelberg, 2006.
[29] W. Biel, et al., Vacuum ultraviolet spectroscopy at TEXTOR, Fus. Sci. Technol. 47 (2005) 246–252.
[30] J.V. Seggern, et al., Long term behaviour of material erosion and deposition on the vessel wall and remote areas of TEXTOR, J. Nuc. Mat. 313-316 (2003) 439–443.
[31] W.R. Wampler, et al., Erosion and deposition of metals and carbon in the DIII-D divertor, J. Nucl. Mater. 233-237 (1996) 791–797.
[32] J. Boedo, et al., Flows in the TEXTOR SOL and edge plasma, J. Nuc. Mat. 196-198 (1992) 489–492.
[33] J. Strachan, et al., Modelling of carbon migration during JET ^{13}C injection experiments, Nucl. Fusion 48 (2008) 105002.
[34] J.P. Coad, et al., Overview of material re-deposition and fuel retention studies at JET with the Gas Box divertor, Nucl. Fusion. 46 (2006) 350.